ISA Transactions xxx (xxxx) xxx–xxx

Contents lists available at ScienceDirect

ISA Transactions

journal homepage: www.elsevier.com/locate/isatrans

Practice article

Dual closed-loop sliding mode control for a decoupled three-link wheeled mobile manipulator

In Seok Seo[a], Seong Ik Han[b,*]

[a] Dept. of Mechanical Engineering, Pusan National University, 63 beon-gil, Busandaehak-ro, Jangjeong-dong, Geumjeong-gu, Busan city, 46241, South Korea
[b] Department of Mechanical System Engineering, Dongguk University Gyeongju, 123-Dongdae-ro, Gyeongju city, Gyeongsangbuk-do, 38066, South Korea

ARTICLE INFO

Keywords:
Kinematic and dynamic model of wheeled mobile manipulator
Sliding mode control
Dual closed-loop control
Assumed feedforward model control
Finite-time sliding mode control

ABSTRACT

This paper presents a dual closed-loop sliding mode control strategy for a wheeled mobile manipulator with three-wheeled mobile platform (WMP) and three-link manipulator. The Euler-Lagrange method combined partially with the Newtonian method is applied to obtain full dynamic model and decoupled model is constructed in order to provide simple dynamic model for controller's structure to be simplified. Instead of the conventional velocity command trajectory based kinematic backstepping control method, a dual closed-loop control system is designed. A virtual velocity command based on sliding mode surface is generated in outer loop and the gap between a generated virtual command velocity and real velocity is compensated by an inner loop sliding mode controller. Outer loop helps to faster posture trajectory generation for locomotion of the WMP. Next, a finite-time sliding mode controller with an assumed feedforward dynamic gain method is designed for joint trajectory tracking for three-link manipulator by adding finite-time control terms in the designed controllers to obtain faster settling time and stronger robustness. The designed controllers were implemented into microprocessor connected to DC and dynamixel motor systems equipped in mobile platform and manipulator, respectively. Comparative simulation and experiment with a conventional sliding mode control show the effectiveness of the proposed dual closed-loop finite time sliding mode control scheme.

1. Introduction

Over the past decades, there have been many studies on wheeled mobile manipulators [1–7], which have become increasingly ubiquitous and are applied to several fields, including hazardous exploration, search and rescue, health-care, manufacturing, and entertainment. A wheeled mobile manipulator is comprised of wheeled mobility configuration and one or more robotic arms mounted on the mobile platform. The combination of platform mobility and arm manipulability increases the ability to perform dexterous robotic works that require both locomotion and manipulation compared to fixed manipulators. However, the configuration of kinematic and dynamic model is complex due to the coupling motion between the wheeled mobile platform (WMP) and manipulator. For kinematic posture control of the WMP, in many cases, the backstepping method [8–12] based on the reference velocity tracking viewpoint has been adopted with consideration of nonholonomic constraint condition. Thus, a desired position command is indirectly generated from the velocity command. This makes intuitive posture generation to be difficult except simple motion case. Depending on this velocity tracking method, when various motion configurations are required, it is difficult to obtain position command directly. If a direct and intuitive posture control command is adopted in the WMP control scheme, the generation of position trajectory can be conveniently and easily generated.

Recently, the dual closed-loop control method combined with sliding mode control (SMC) [13–17] has been developed in the aero vehicle control and servo systems [17] [18], where the kinematic and kinetic control loop were separated as the outer and inner loops, respectively and two loop controllers for each loop were constructed. By borrowing this concept, we apply this dual closed-loop SMC to posture control of the WMP system. As an outer loop control system, a kinematic control system is constructed such that a position reference command is directly chosen and virtual velocity command is designed to generate the target velocity of the dynamic controller of the WMP. Next, an inner loop controller is built such that coupling effect transferred from manipulator motion as well as the dynamic effect of mobile platform are compensated by a designed sliding mode controller. This control can provide more intuitive position tracking target and is more

* Corresponding author. Department of Mechanical System Engineering, Dongguk University Gyeongju, 123-Dongdae-ro, Gyeongju city, Gyeongsangbuk-do, 38066, South Korea.
E-mail addresses: 76024515@naver.com (I.S. Seo), skhan@dongguk.ac.kr (S.I. Han).

https://doi.org/10.1016/j.isatra.2018.07.023
Received 20 June 2017; Received in revised form 27 June 2018; Accepted 19 July 2018

conveniently used in the WMP motion control than the conventional velocity command based backstepping posture control method [8–12].

Dynamics of the whole system including both three-wheeled WMP and three-link manipulator are modeled using Euler-Lagrange equation with consideration of kinematic and kinetic relations of each component. Next, decoupled dynamic equations are built to avoid heavy controller structure and make controller to be designed easily. The sliding mode controllers for each loop are designed and a feedforward model obtained from iterative parameter assuming process is considered in the controller to bypass complex parameters identification of the mobile manipulator system. For comparing with the proposed dual closed-loop finite-time SMC system, the conventional first-order sliding mode controller with dual closed-loop is designed. Moreover, by adopting robust SMC scheme with additional finite-time control terms, which guarantee faster settling time and stronger robustness in the mobile manipulator system, more robust control performance against uncertainty of coupling effect between mobile platform navigation and variation of manipulator working condition can be obtained. The stability analysis for the closed-loop system with these control terms is conducted and finite-time is induced by the finite-time control theorem [19,20]. Furthermore, unlike the conventional terminal SMC [21], a proposed finite-time control can void the singularity problem of the conventional terminal SMC without introducing the terminal sliding mode surface.

Next, the designed control systems were implemented into the designed ARM microprocessor control board combined with the mobile robot DC motor drive system and dynamixel motor system [22] in the manipulator to execute experimental performance verification.

The main contributions of this study are summarized as follows: 1) the full dynamic model of the wheeled mobile manipulator is constructed and its model is decoupled as two parts. 2) By generating virtual velocity command, an outer loop SMC is designed to provide more intuitive posture tracking trajectory of the WMP than the conventional velocity tracking method. 3) An inner loop robust sliding mode controller is designed to guarantee finite-time convergence with an assumed dynamic parameter method that can give fast controller design without depending on tedious parameter identification. 4) Faster convergence time and stronger robustness are obtained by only considering finite-time control terms in the designed sliding mode controllers.

Application examples of simulation and experiment were presented for verification of the proposed method with comparison of the conventional sliding mode control.

2. Problem formulation

2.1. Dynamic model of three-wheeled mobile manipulators

We made a three-wheeled mobile manipulator system as shown in Fig. 1. The mobile robot has three wheels with two driving wheel in left and right sides and passive wheel in the front part. The manipulator has three links and 3° of freedom, where each rotation axis is equipped with dynamixel motor. The dynamic equations of a three-wheeled mobile manipulator system are derived using the Euler-Lagrange equation according to the kinematics and force relations of Fig. 1. The derived dynamics are modified from the relationship of forces acting on the body and links, and constraints between the wheel and contact surface without considering the Lagrange multiplier method, which is used to solve the nonholonomic constraint problems of mobile robots. The variable of three-wheeled mobile manipulator are defined as follows: τ_r, τ_l, τ_1, τ_2, and τ_3 are the torque acting on two wheels, joint 1, 2, and 2, respectively, θ_r and θ_l are the rotation angle of the left and right wheel of the mobile platform; R and φ are the forward traveled position and the rotation angle of the mobile platform; v and ω are the forward traveled velocity and the rotation velocity of the mobile platform; θ_1, θ_2, and θ_3 are the rotation angles of links 1, 2, and 3 with respect to z_0, z_1, and z_2 axes; m_p, m_w, m_1, m_2, m_3 are the mass of the mobile platform, wheel, link 1, and link 2; I_z and I_{zw} are the moment of inertia of the mobile platform and wheel with respect to z_0 axis; d is the distance between point P and wheels; r is the radius of the wheels; l_1, l_2, and l_3 are the lengths of link 1, link 2, and link 3; and r_2 and r_3 are the distance between joints and the center of mass of the links.

Forces and torques acting on the body and each link are described in Fig. 2 and the tire dynamic relations are illustrated in Fig. 3 where F_r and F_l are the force interacting between the left and right wheels; T_r and T_l are the torque generated in the left and right wheels; F_{fr} and F_{fl} are the friction force interacting between the wheels and the contact surface. The position of C, the center of mass of the mobile platform are given as x and y. The position of the center of mass for two wheels are given by

$$
\begin{aligned}
x_r &= x + d\sin\varphi,\\
y_r &= y - d\cos\varphi,\\
x_l &= x - d\sin\varphi,\\
y_l &= y + d\cos\varphi,
\end{aligned}
\tag{1}
$$

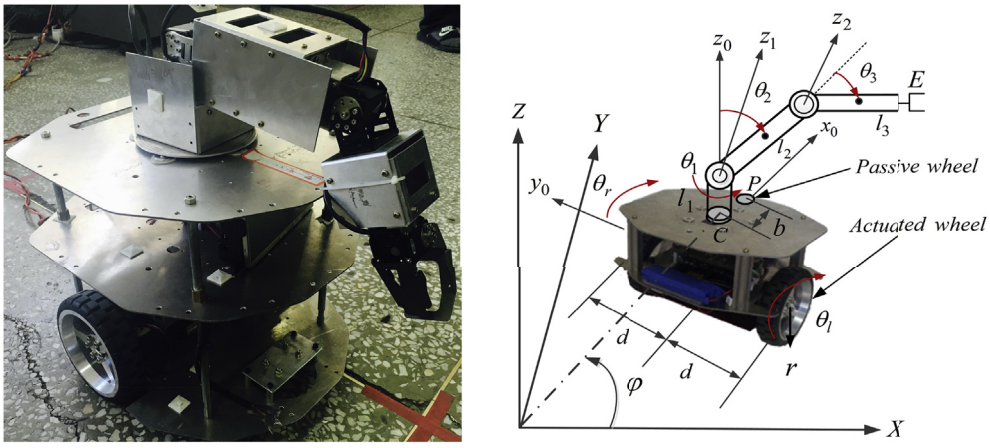

Fig. 1. Photograph and schematic description of the designed mobile manipulator.

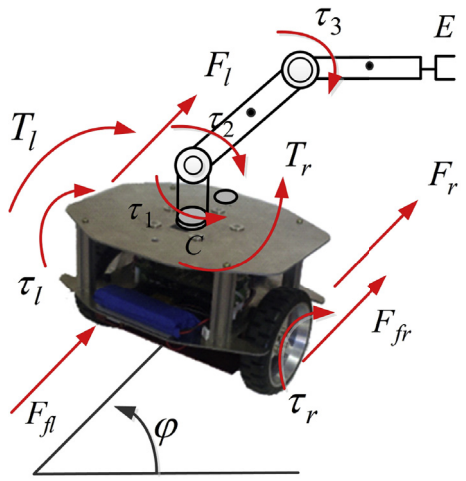

Fig. 2. Force and torque acting on the body.

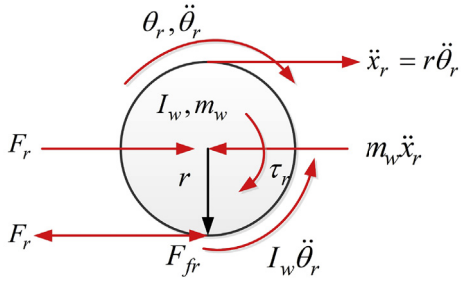

Fig. 3. Force and torque acting on the wheel.

Letr_1, r_2, and $r_3$denote the distance between joints and the center of mass of links. The coordinates of the center of mass of link1, link2, and link3 can be given as

$$x_1 = x,$$

$$y_1 = y,$$

$$x_2 = x + r_2 \sin\theta_2 \cos(\varphi + \theta_1),$$

$$y_2 = y + r_2 \sin\theta_2 \sin(\varphi + \theta_1),$$

$$x_3 = x + l_2 \sin\theta_2 \cos(\varphi + \theta_1) + r_3 \sin(\theta_2 + \theta_3)\cos(\varphi + \theta_1),$$

$$y_3 = y + l_2 \sin\theta_2 \sin(\varphi + \theta_1) + r_3 \sin(\theta_2 + \theta_3)\sin(\varphi + \theta_1). \quad (2)$$

The kinematic energy is expressed as follows:

$$\begin{aligned} T &= \tfrac{1}{2}m_p(\dot{x}^2 + \dot{y}^2) + \tfrac{1}{2}I_\varphi\dot{\varphi}^2 + \tfrac{1}{2}I_{z0}(\dot{\varphi} + \dot{\theta}_1)^2 \\ &+ \tfrac{1}{2}m_2[\dot{x} - r_2\dot{\theta}_2 s\theta_2 c(\varphi + \theta_1) - r_2(\dot{\varphi} + \dot{\theta}_1)c\theta_2 s(\varphi + \theta_1)]^2 \\ &+ \tfrac{1}{2}m_2[\dot{y} - r_2\dot{\theta}_2 s\theta_2 s(\varphi + \theta_1) + r_2(\dot{\varphi} + \dot{\theta}_1)c\theta_2 c(\varphi + \theta_1)]^2 \\ &+ \tfrac{1}{2}I_{z1}[(\dot{\varphi} + \dot{\theta}_1)^2 + \dot{\theta}_2^2] \\ &+ \tfrac{1}{2}m_3\begin{bmatrix} \dot{x} - l_2\dot{\theta}_2 s\theta_2 c(\varphi + \theta_1) - l_2(\dot{\varphi} + \dot{\theta}_1)c\theta_2 s(\varphi + \theta_1) \\ -r_3\dot{\theta}_{23} s\theta_{23} c(\varphi + \theta_1) - r_3(\dot{\varphi} + \dot{\theta}_1)c\theta_{23} s(\varphi + \theta_1) \end{bmatrix}^2 \\ &+ \tfrac{1}{2}m_3\begin{bmatrix} \dot{y} - l_2\dot{\theta}_2 s\theta_2 s(\varphi + \theta_1) + l_2(\dot{\varphi} + \dot{\theta}_1)c\theta_2 c(\varphi + \theta_1) \\ -r_3\dot{\theta}_{23} s\theta_{23} s(\varphi + \theta_1) + r_3(\dot{\varphi} + \dot{\theta}_1)c\theta_{23} c(\varphi + \theta_1) \end{bmatrix}^2 \\ &+ \tfrac{1}{2}I_{z2}[(\dot{\varphi} + \dot{\theta}_1)^2 + \dot{\theta}_{23}^2], \end{aligned} \quad (3)$$

where $m_p = m_b + m_1$, $s\theta = \sin\theta$, $c\theta = \cos\theta$, and$\theta_{ij} = \theta_i + \theta_j$. The potential energy is obtained as follows:

$$V = m_2 g r_2 s\theta_2 + m_3 g(l_2 s\theta_2 + r_3 s\theta_{23}). \quad (4)$$

By defining Lagrangian $L = T - V$and using the Euler-Lagrange equation$\frac{d}{dt}\left(\frac{\partial L}{\partial \dot{q}}\right) - \frac{\partial L}{\partial q} = Q$, the system dynamics subject to nonholonomic constraint is formulated as

$$M(q)\ddot{q} + C(q, \dot{q})\dot{q} + G(q) + \tau_d = B\tau - A_0^T\lambda, \quad (5)$$

where$q = [x\ y\ \varphi\ \theta_1\ \theta_2\ \theta_3]^T$is a generalized coordinate; $M(q)$is a symmetric and positive definite inertia matrix; $C(q, \dot{q})$is a matrix of velocity-dependent centripetal and Coriolis forces; $G(q)$is a gravitational vector; $\tau_d$is a bounded unknown disturbance including unmodelled dynamics and exogenous disturbance; $B$is the input transformation matrix; $\tau$is an input torque vector; $A_o^T = [A^T\ \ 0]^T A$is a vector related to nonholonomic condition of WMP defined in (17); and$\lambda$is the Lagrange multiplier.

The tire dynamics from Fig. 3 are given as.

$$m_r\ddot{x}_r = -F_r + F_{fr},$$

$$m_l\ddot{x}_l = -F_l + F_{fl}, \quad (6)$$

$$I_w\ddot{\theta}_r = \tau_r - rF_{fr},$$

$$I_w\ddot{\theta}_l = \tau_l - rF_{fl}, \quad (7)$$

where $m_r = m_l = m_w$, $F_r$and$F_l$are traction force, and$F_{fr}$and$F_{fl}$are friction force. Then, based on (6) and (7), we obtain

$$F_r = \frac{\tau_r}{r} - \frac{I_w\ddot{\theta}_r}{r} - m_w\ddot{x}_r,$$

$$F_l = \frac{\tau_l}{r} - \frac{I_w\ddot{\theta}_l}{r} - m_w\ddot{x}_l, \quad (8)$$

The relationship between$\ddot{\theta}_r = \ddot{x}_r/rand\ddot{\theta}_l = \ddot{x}_l/r$are provided if a slip does not occur between tire and contact surface. Using the force and torque relationships of Fig. 3, (8) can be expressed as the following forces and torques:

$$F_r = \frac{\tau_r}{r} - \left(\frac{I_w}{r^2} + m_w\right)\ddot{x}_r,$$

$$F_l = \frac{\tau_l}{r} - \left(\frac{I_w}{r^2} + m_w\right)\ddot{x}_l. \quad (9)$$

$$T_r = dF_r,$$

$$T_l = dF_l. \quad (10)$$

Under the assumption of no sideslip, the relationship between$\ddot{x} = \frac{\ddot{x}_l + \ddot{x}_r}{2}c\varphi\ddot{y} = \frac{\ddot{x}_l + \ddot{x}_r}{2}s\varphi$, $\dot{\varphi} = \frac{r}{2d}(\dot{\theta}_r - \dot{\theta}_l) = \frac{\dot{x}_r - \dot{x}_l}{2d}$, and$\ddot{\varphi} = \frac{r}{2d}(\ddot{\theta}_r - \ddot{\theta}_l) = \frac{\ddot{x}_r - \ddot{x}_l}{2d}$can be obtained. These relationships with considering (9) and (10) yield

$$\begin{aligned} (F_r + F_l)c\varphi &= \tfrac{\tau_r + \tau_l}{r}c\varphi - \left(\tfrac{I_w}{r^2} + m_w\right)(\ddot{x}_l + \ddot{x}_r)c\varphi \\ &= \tfrac{\tau_r + \tau_l}{r}c\varphi - 2\left(\tfrac{I_w}{r^2} + m_w\right)\ddot{x}, \end{aligned} \quad (11)$$

$$\begin{aligned} (F_r + F_l)s\varphi &= \tfrac{\tau_r + \tau_l}{r}s\varphi - \left(\tfrac{I_w}{r^2} + m_w\right)(\ddot{x}_l + \ddot{x}_r)s\varphi \\ &= \tfrac{\tau_r + \tau_l}{r}s\varphi - 2\left(\tfrac{I_w}{r^2} + m_w\right)\ddot{y}, \end{aligned} \quad (12)$$

$$\begin{aligned} T_\varphi = T_r - T_l &= \frac{d(\tau_r - \tau_l)}{r} - d\left(\frac{I_w}{r^2} + m_w\right)(\ddot{x}_r - \ddot{x}_l) \\ &= \frac{d}{r}(\tau_r - \tau_l) - 2d^2\left(\frac{I_w}{r^2} + m_w\right)\ddot{\varphi}. \end{aligned} \quad (13)$$

Considering the above relationships, the dynamic matrices and vectors given in (5) can be expressed as the following decoupled form:

$$\begin{bmatrix} M_v & M_{vm} \\ M_{mv} & M_m \end{bmatrix}\begin{bmatrix} \ddot{q}_v \\ \ddot{q}_m \end{bmatrix} + \begin{bmatrix} C_v & C_{vm} \\ C_{mv} & C_m \end{bmatrix}\begin{bmatrix} \dot{q}_v \\ \dot{q}_m \end{bmatrix} + \begin{bmatrix} 0 \\ G_m \end{bmatrix} + \begin{bmatrix} \tau_{dv} \\ \tau_{dm} \end{bmatrix} = \begin{bmatrix} B_v & 0 \\ 0 & B_m \end{bmatrix}\begin{bmatrix} \tau_v \\ \tau_m \end{bmatrix} - \begin{bmatrix} A^T\lambda \\ 0 \end{bmatrix}. \quad (14)$$

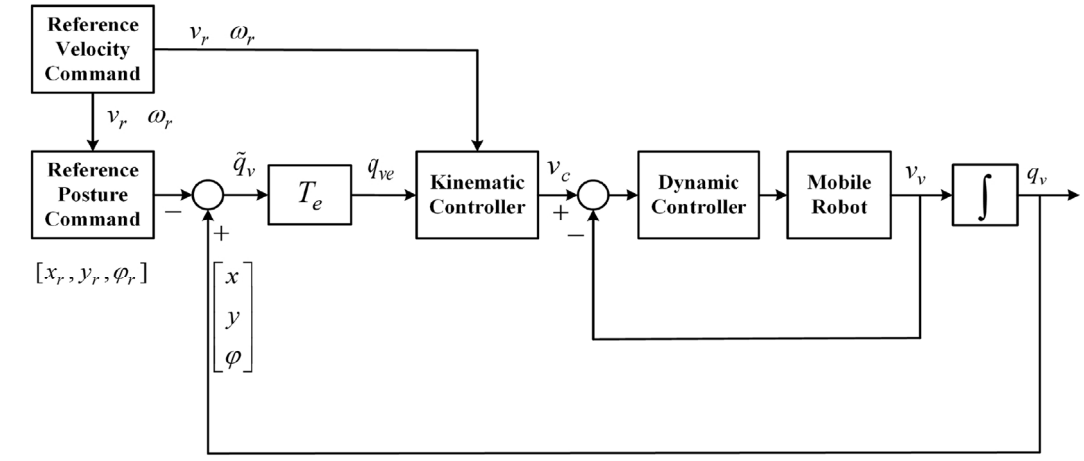

(a) The conventional posture control system for the WMP

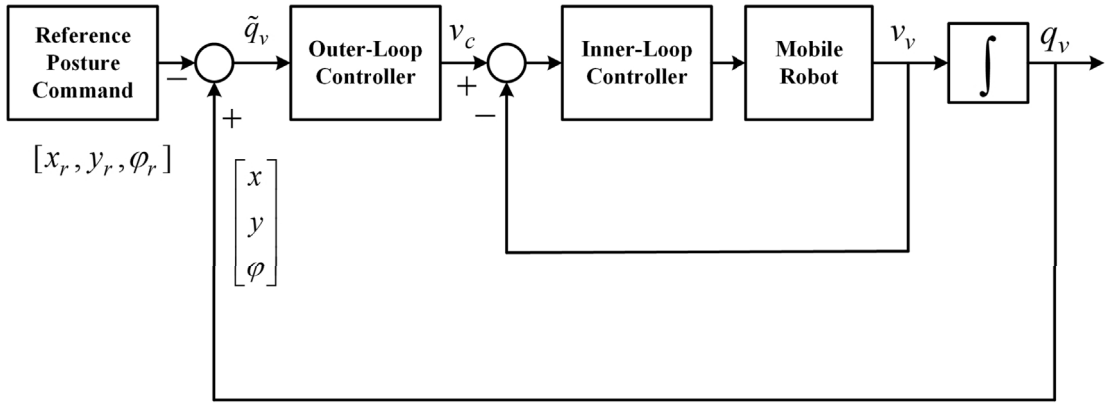

(b) The proposed dual closed-loop posture control system

Fig. 4. Block diagram of the posture control system for the WMP.

where

$$M(q) = \begin{bmatrix} M_v & M_{vm} \\ M_{mv} & M_m \end{bmatrix}, C(q, \dot{q}) = \begin{bmatrix} C_v & C_{vm} \\ C_{mv} & C_m \end{bmatrix}, G(q) = \begin{bmatrix} 0 \\ G_m \end{bmatrix},$$

$$B = \begin{bmatrix} c\varphi/r & c\varphi/r & 0 & 0 & 0 \\ s\varphi/r & s\varphi/r & 0 & 0 & 0 \\ d/r & -d/r & 0 & 0 & 0 \\ 0 & 0 & 1 & 0 & 0 \\ 0 & 0 & 0 & 1 & 0 \\ 0 & 0 & 0 & 0 & 1 \end{bmatrix} = \begin{bmatrix} B_v & 0_{3\times3} \\ 0_{2\times3} & B_m \end{bmatrix},$$

$$\tau_d = [\tau_{dx} \ \ \tau_{dy} \ \ \tau_{d\varphi} \ \ \tau_{d1} \ \ \tau_{d2} \ \ \tau_{d3}]^T = [\tau_{dv} \ \ \tau_{dm}]^T, \tau = [\tau_r \ \ \tau_l \ \ \tau_1 \ \ \tau_2 \ \ \tau_3]^T = [\tau_v \ \ \tau_m]^T.$$

$$M_v = \begin{bmatrix} M_{xx} & 0 & M_{x\varphi} \\ 0 & M_{yy} & M_{y\varphi} \\ M_{\varphi x} & M_{\varphi y} & M_{\varphi\varphi} \end{bmatrix}, M_{vm} = \begin{bmatrix} M_{x\theta_1} & M_{x\theta_2} & M_{x\theta_3} \\ M_{y\theta_1} & M_{y\theta_2} & M_{y\theta_3} \\ M_{\varphi\theta_1} & M_{\varphi\theta_2} & M_{\varphi\theta_3} \end{bmatrix}, M_{mv} = \begin{bmatrix} M_{\theta_1 x} & M_{\theta_1 y} & M_{\theta_1\varphi} \\ M_{\theta_2 x} & M_{\theta_2 y} & M_{\theta_2\varphi} \\ M_{\theta_3 x} & M_{\theta_3 y} & M_{\theta_3\varphi} \end{bmatrix},$$

$$M_m = \begin{bmatrix} M_{\theta_1\theta_1} & 0 & 0 \\ 0 & M_{\theta_2\theta_2} & M_{\theta_2\theta_3} \\ 0 & M_{\theta_3\theta_2} & M_{\theta_3\theta_3} \end{bmatrix}, C_v = \begin{bmatrix} 0 & 0 & C_{x\varphi} \\ 0 & 0 & C_{y\varphi} \\ C_{\varphi x} & 0 & C_{\varphi\varphi} \end{bmatrix}, C_{vm} = \begin{bmatrix} C_{x\theta_1} & C_{x\theta_2} & C_{x\theta_1} \\ C_{y\theta_1} & C_{y\theta_2} & C_{y\theta_3} \\ C_{\varphi\theta_1} & C_{\varphi\theta_2} & C_{\varphi\theta_3} \end{bmatrix},$$

$$C_{mv} = \begin{bmatrix} C_{\theta_1 x} & C_{\theta_1 y} & C_{\theta_1\varphi} \\ C_{\theta_2 x} & 0 & C_{\theta_2\varphi} \\ C_{\theta_3 x} & 0 & C_{\theta_3\varphi} \end{bmatrix}, C_m = \begin{bmatrix} C_{\theta_1\theta_1} & C_{\theta_1\theta_2} & C_{\theta_1\theta_3} \\ C_{\theta_2\theta_1} & C_{\theta_2\theta_2} & C_{\theta_2\theta_3} \\ C_{\theta_3\theta_1} & C_{\theta_3\theta_2} & C_{\theta_3\theta_3} \end{bmatrix}, B_v = \begin{bmatrix} c\varphi/r & c\varphi/r \\ s\varphi/r & s\varphi/r \\ d/r & -d/r \end{bmatrix}, B_m = \begin{bmatrix} 1 & 0 & 0 \\ 0 & 1 & 0 \\ 0 & 0 & 1 \end{bmatrix},$$

$\tau_{dv} = [\tau_{dx} \ \ \tau_{dy} \ \ \tau_{d\varphi}]$, $\tau_{dm} = [\tau_{d1} \ \ \tau_{d2} \ \ \tau_{d3}]$, $\tau_v = [\tau_r \ \ \tau_l]^T$, and $\tau_m = [\tau_1 \ \ \tau_2 \ \ \tau_3]^T$.

Property 1. The inertia matrices M are symmetric, positive definite, and bounded. The norms of $C(q, \dot{q})$ are also bounded.

Property 2. The matrices $\dot{M}(q) - 2C(q, \dot{q})$ are skew-symmetric because of the suitable definition of the corresponding inertia and Coriolis matrix.

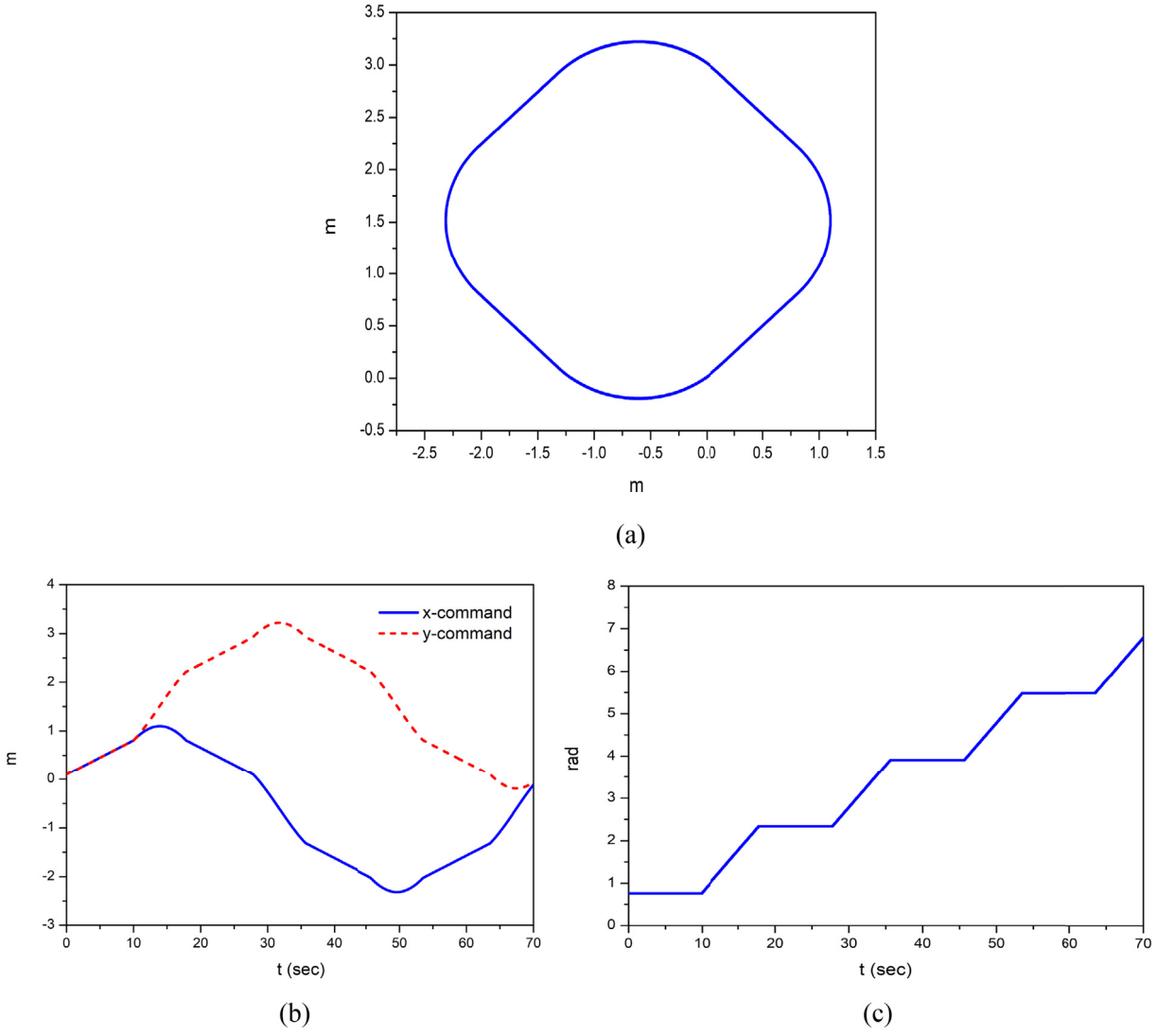

Fig. 5. The generated motion command of the WMP system. (a) Linear and rotary command motion. (b). Command motions in x and y directions. (c) Command angle.

3. Design the dual closed-loop sliding mode controller of three-link mobile manipulator and stability analysis

3.1. Kinematics of the mobile platform

The WMP system has three degrees of freedom as$q_v = [x \;\; y \;\; \varphi]^T$. The velocity relation of the WMP is given as

$$\dot{q}_v = \begin{bmatrix} \dot{x} \\ \dot{y} \\ \dot{\varphi} \end{bmatrix} = \begin{bmatrix} \cos\varphi & 0 \\ \sin\varphi & 0 \\ 0 & 1 \end{bmatrix} \begin{bmatrix} v_l \\ \omega \end{bmatrix} = J_v(\varphi)v. \tag{15}$$

where$v_l(t) \in R$denotes the linear velocity of the point C of the WMP, $\omega(t) \in R$denotes the angular velocity of the point C of the WMP, and $J_v(\varphi)$is a transformation matrix which transforms velocities v in mobile coordinates to velocities $\dot{q}_v$in Cartesian coordinates. The nonholonomic velocity constraint declares that driving wheels purely roll and do not slip. In the other words, the WMP can only move in a direction, which is normal to the axis of the driving wheels,

$$\dot{y}\cos\varphi - \dot{x}\sin\varphi = 0, \tag{16}$$

$$A^T(q_v)\dot{q}_v = 0, \tag{17}$$

where$A^T(q_v) = [-\sin\varphi \;\; \cos\varphi \;\; 0]^T$.

3.2. Design of the kinematic baskstepping controller for the WMP

Traditionally, the kinematic backstepping control has been frequently applied to posture control for the WMP system. We illustrate briefly this method. A reference of the WMP that generates a trajectory for the actual one to follow:

$$\dot{q}_{vr} = J_v(\varphi_r)v_r, \tag{18}$$

where$q_{vr} = [x_r \;\; y_r \;\; \varphi_r]^T \in R^3$denotes the desired time-varying position and orientation trajectory, and$v_r = [v_{lr} \;\; \omega_r]^T \in R^2$ denotes the reference time-varying linear and angular velocity. In real application, $v_r$and its derivative are known and bounded. It is necessary to find the appropriate velocity control law$v_c = [v_{lc} \;\; \omega_c]^T$, such that$q_v \to q_{vr}ast \to \infty$. The trajectory tracking problem is to track a reference mobile robot with a postureq_{vr}. Therefore, we define tracking error between the actual and desired posture:

$$\tilde{q}_v = q_v - q_r = \begin{bmatrix} x - x_r \\ y - y_r \\ \varphi - \varphi_r \end{bmatrix}. \tag{19}$$

The posture tracking error is then obtained as follows:

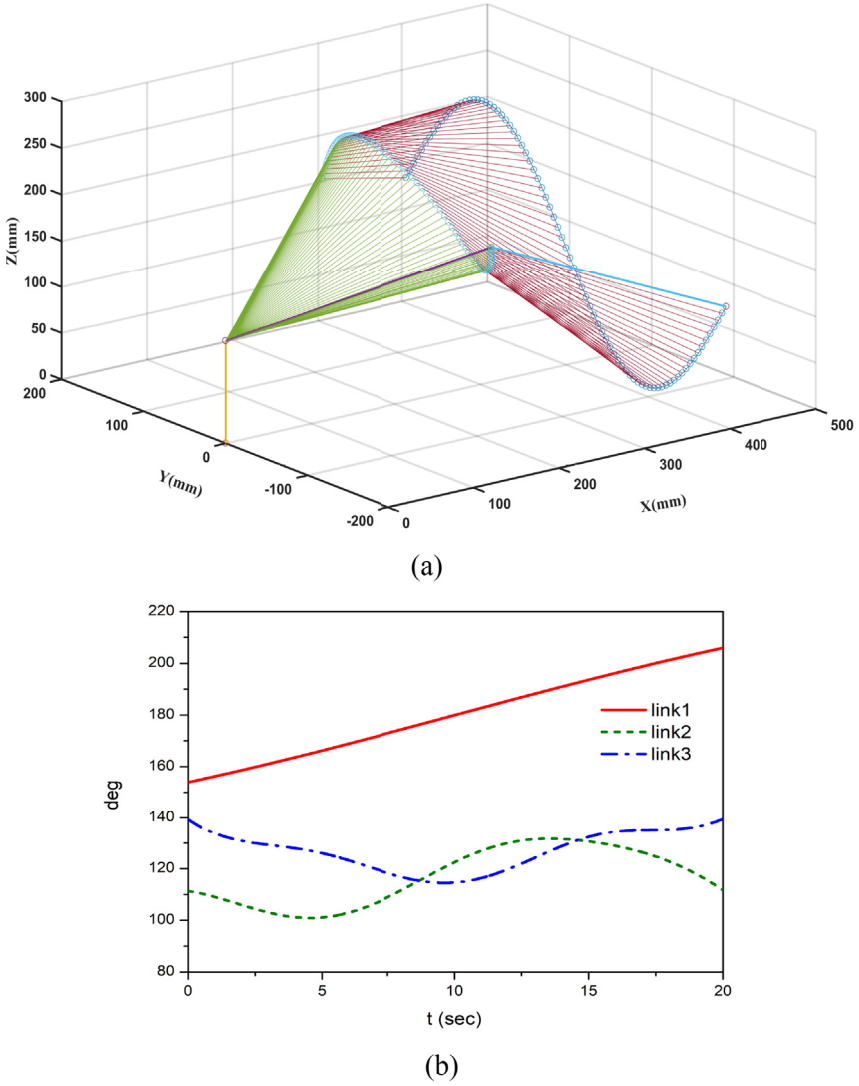

Fig. 6. The generated command motion for the manipulator. (a) The motions of the end-effector and each joint. (b) Joint motions.

$$q_{ve} = \begin{bmatrix} e_{v1} \\ e_{v2} \\ e_{v3} \end{bmatrix} = \begin{bmatrix} \cos\varphi & \sin\varphi & 0 \\ -\sin\varphi & \cos\varphi & 0 \\ 0 & 0 & 1 \end{bmatrix} \begin{bmatrix} x - x_r \\ y - y_r \\ \varphi - \varphi_r \end{bmatrix}. \tag{20}$$

From the relations of (15), (18), and (20), we have

$$\dot{q}_{ve} = \begin{bmatrix} \dot{e}_{v1} \\ \dot{e}_{v2} \\ \dot{e}_{v3} \end{bmatrix} = v_l \begin{bmatrix} 1 \\ 0 \\ 0 \end{bmatrix} + \omega \begin{bmatrix} e_{v2} \\ -e_{v1} \\ -1 \end{bmatrix} + \begin{bmatrix} -v_{lr}\cos e_{v3} \\ v_{lr}\sin e_{v3} \\ \omega_r \end{bmatrix}. \tag{21}$$

The target or command velocity using backstepping method is given as

$$v_c = \begin{bmatrix} v_{lc} \\ \omega_c \end{bmatrix} = \begin{bmatrix} -k_{v1}e_{v1} + v_{lr}\cos e_{v3} \\ \omega_r - k_{v2}v_{lr}e_{v2} - k_{v3}v_{lr}\sin e_{v3} \end{bmatrix}, \tag{22}$$

where k_{v1}, k_{v2} and k_{v3} are positive constants and $v_{lr} > 0$. This is called the kinematic control. If the perfect velocity tracking is achieved as

$$v_c = \begin{bmatrix} v_{lc} \\ \omega_c \end{bmatrix} = \begin{bmatrix} v_l \\ \omega \end{bmatrix} = v_v, \tag{23}$$

then the kinematic model is asymptotically stable with respect to the reference trajectory: $q_{ve} = [e_{v1} \quad e_{v2} \quad e_{v3}]^T \to 0$ as $t \to \infty$.

3.3. Design outer closed-loop kinematic sliding mode controller for the WMP

We define tracking error between the actual and desired posture:

$$q_{ve} = q_v - q_{vc} = \begin{bmatrix} x - x_c \\ y - y_c \\ \varphi - \varphi_c \end{bmatrix}. \tag{24}$$

The sliding surface of the outer loop of the mobile platform is defined as

$$s_{vo} = q_{ve} + k_{voe}\int_0^t q_{ve}\,dt, \tag{25}$$

where $k_{voe} = diag(k_{voex}, k_{voey}, k_{voe\varphi}) > 0$ is a gain matrix. Taking the virtual velocity command v_{vc} as the virtual control of the velocity v_v of the mobile platform instead of the command velocity in (22), we have

$$\dot{q}_v = J_v(\varphi)v_{vc}. \tag{26}$$

To satisfy the stability condition, which will be given in Section 3, we define

$$\dot{s}_{vo} = -k_{vo1}s_{vo} - k_{vo2}\frac{s_{vo}}{|s_{vo}| + \varepsilon_{vo}} - k_{vo3}sig(s_{vo})^{\gamma_{vo}}, \tag{27}$$

where $k_{voj} = diag(k_{vojx}, k_{vojy}, k_{voj\varphi}) > 0$, $j = 1,2,3$, are gain matrices, $\varepsilon_{vo} > 0$ and $0 < \gamma_{vo} < 1$ are constants, and $sig(s_{vo})^{\gamma_{vo}} = |s_{vo}|^{\gamma_{vo}} sign(s_{vo})$. We then obtain the following result:

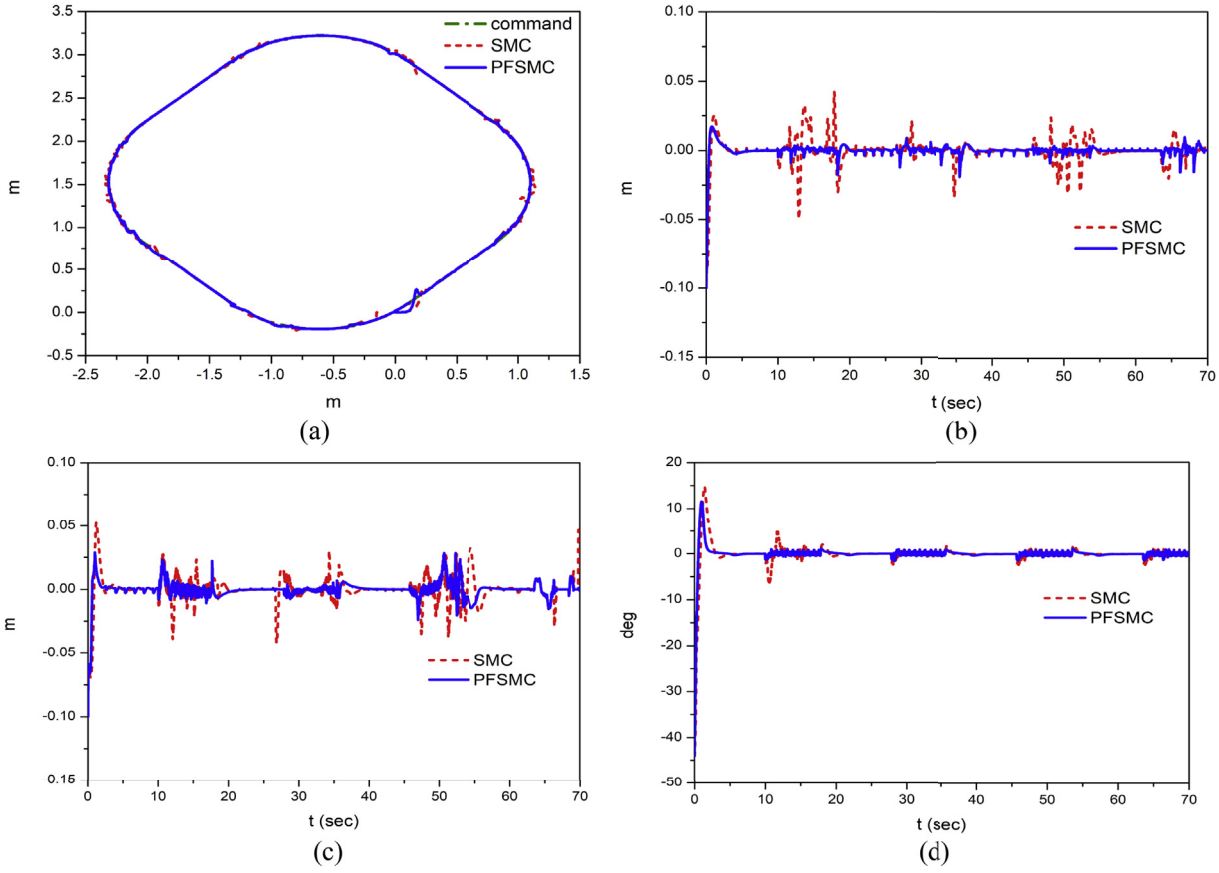

Fig. 7. Simulation results of the WMP for the linear and rotational motion command input of the SMC and. PFSMC systems: (a) Position tracking output. (b) X-direction tracking error. (c) Y-direction tracking error. (d) Angular tracking error.

$$\begin{aligned}\dot{s}_{vo} &= \dot{q}_{ve} + k_{voe}q_{ve}\\ &= \dot{q}_v - \dot{q}_{vc} + k_{voe}q_{ve}\\ = J_v(\varphi)v_{vc} - \dot{q}_{vc} + k_{voe}q_{ve} &= -k_{vo1}s_{vo} - k_{vo2}\frac{s_{vo}}{|s_{vo}| + \varepsilon_{vo}} - k_{vo3}sig(s_{vo})^{\gamma_{vo}}.\end{aligned} \tag{28}$$

A finite time outer loop controller is obtained from (28) as follows:

$$v_{vc} = J_v^{+}(\varphi)\left(\dot{q}_{vc} - k_{voe}q_{ve} - k_{vo1}s_{vo} - k_{vo2}\frac{s_{vo}}{|s_{vo}| + \varepsilon_{vo}} - k_{vo3}sig(s_{vo})^{\gamma_{vo}}\right), \tag{29}$$

where $J_v^{+}(\varphi) = (J_v^T(\varphi)J_v(\varphi))^{-1}J_v^T(\varphi)$ is the pseudo inverse of $J_v(\varphi)$.

Remark 1. In the outer loop controller given in (29), it is well known that the controller term of the sigmoid function $s_{vo}/(|s_{vo}| + \varepsilon_{vo})$, is related to the disturbance rejection performance. If $\varepsilon_{vo} \to 0$, this term becomes the sign function, which leads to more rigorous disturbance rejection performance but more chattering appears in control input. The controller term $-k_{vo3}sig(s_{vo})^{\gamma_{vo}}$, guarantees fast settling time and provides more improved disturbance rejection performance indirectly like the terminal sliding scheme [21]. This property will be proved in the Lyapunov stability theorem.

3.4. Design of the inner loop dynamic sliding mode controller for the WMP

In (14), the mobile dynamics is separated as follows:

$$M_v\ddot{q}_v + C_v\dot{q}_v + F_{dv} = B_v\tau_v - A^T\lambda \tag{30}$$

where $F_{dv} = M_{vm}\ddot{q}_m + C_{vm}\dot{q}_m + \tau_{dv}$. From (18), we have $\ddot{q}_v = J_v\dot{v}_v + \dot{J}_v v_v$. Therefore, (30) can be written as

$$M_vJ_v\dot{v}_v + (M_v\dot{J}_v + C_vJ_v)v_v + F_{dv} = B_v\tau_v - A^T\lambda. \tag{31}$$

Because of $J_v^T(q_v)A^T(q_v) = 0$, multiplying $J_v^T(q_v)$ into the left side of (31) gives

$$M_v'\dot{v}_v + C_v'v_v + F_{dv}' = B_v'\tau_v, \tag{32}$$

where $M_v' = J_v^T(q_v)M_vJ_v$, $C_v' = J_v^T(M_v\dot{J}_v + C_vJ_v)$, $F_{dv}' = J_v^TF_{dv}$, and $B_v' = J_v^TB_v = \begin{bmatrix}1/r & 1/r\\ d/r & -d/r\end{bmatrix}$.

Next, a finite-time sliding mode controller is designed with assumed model feedforwarding technique.

Assumption 1. There are positive real numbers, K_{mv}, K_{cv}, and K_{dv} that satisfy the following conditions:

$$\begin{cases}\|M_v'\| \le K_{mv}\\ \|C_v'\| \le K_{cv},\\ \|F_{dv}'\| \le K_{dv}\end{cases} \tag{33}$$

where $K_{mv} \in R^{2\times2}$ and $K_{cv} \in R^{2\times2}$ are positive finite diagonal matrices and $K_{dv} \in R^2$ is a positive vector, which are determined through trial and error method.

Assumption 2. There are positive real numbers, Δ_{mv}, Δ_{cv}, and Δ_{dv} that satisfy the following conditions:

$$\begin{cases}\|K_{mv} - M_v'(q_v)\| \le \Delta_{mv}\\ \|K_{cv} - C_v'(q_v, \dot{q}_v)\| \le \Delta_{cv},\\ \|K_{dv} - F_{dv}'\| \le \Delta_{dv}\end{cases} \tag{34}$$

where $\Delta_{mv}\Delta_{cv}$, and Δ_{dv} include the assumed error and off-diagonal coupled dynamics of each parameter.

The auxiliary tracking error and command error are defined as

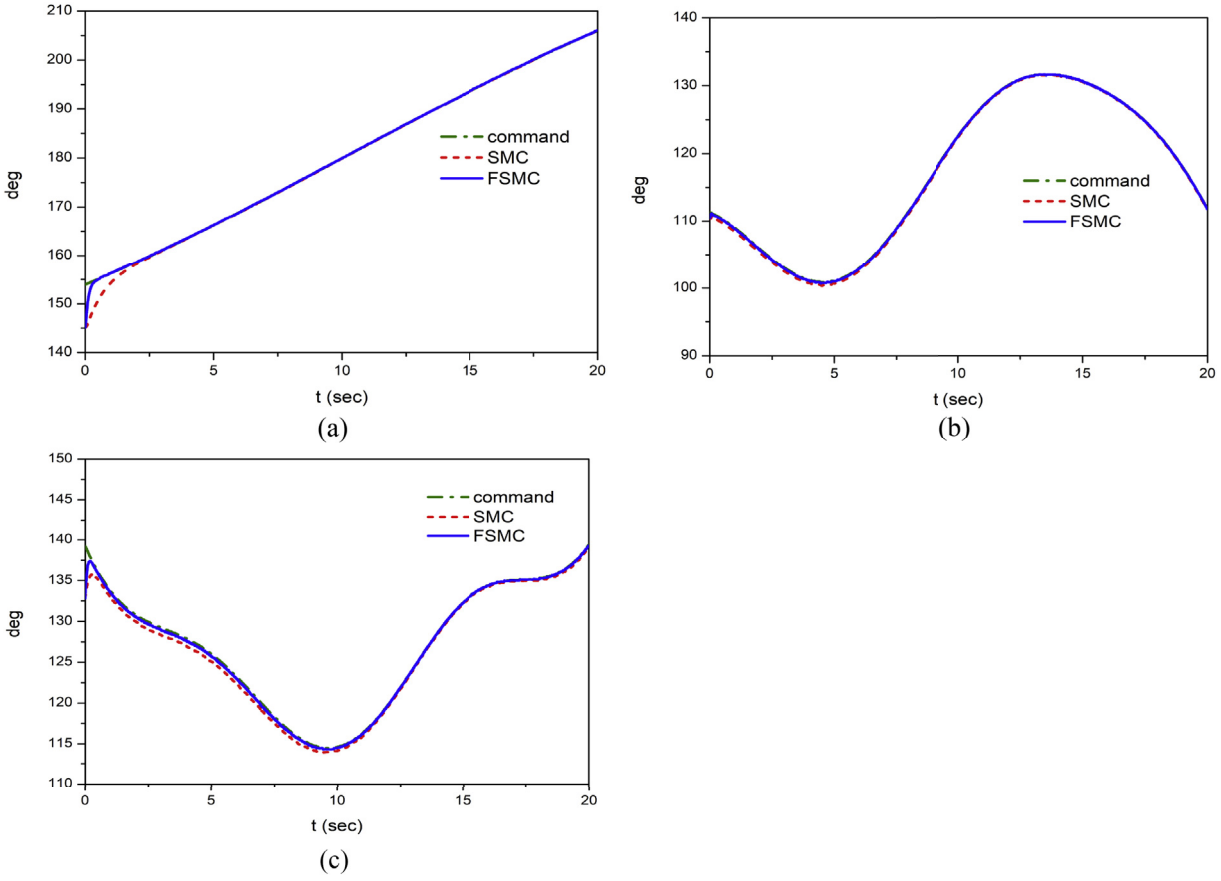

Fig. 8. Simulation results for manipulator of the SMC and PFSMC systems for the change of mass in link 3. (a) Joint 1 angle tracking result. (b) Joint 2 tracking result. (c) Joint 3 tracking result.

follows:

$$e_{vi} = v_v - v_{vc}, \tag{35}$$

$$r_{vi} = v_{vc} - \Lambda_{vi}\int_0^t e_{vi}d\tau, \tag{36}$$

where$e_v = [e_{vv},\ \ e_\omega]^T v_{vc} = [v_{cv},\ v_{c\omega}]^T$ is the desired trajectory, $\Lambda_{vi} = diag(\Lambda_{vv},\Lambda_{v\omega}) > 0$is a constant matrix. The filtered second-order error surface is chosen as

$$s_{vi} = v_v - r_{vi}, \tag{37}$$

The dynamic equation (32) with (37) can be written as

$$\begin{aligned} M_v'\dot{s}_{vi} &= M_v'\dot{v}_v - M_v'\dot{r}_{vi} \\ &= -M_v'\dot{r}_v - C_v'v_v - F_{dv}' + B_v'\tau_v \\ &= -M_v'\dot{r}_v - C_v'r_v - F_{dv}' + B_v'\tau_v - C_v's_v. \end{aligned} \tag{38}$$

We select the dynamic control law$\tau_{vi}$to satisfy the stability condition, which is given in Section 3, as

$$\tau_{vi} = B_v^{-1}\left[-k_{vi1}s_{vi} + \Xi_v^T\phi_v - k_{vi2}\frac{s_{vi}}{|s_{vi}| + \varepsilon_{vi}} - k_{vi3}sig(s_{vi})^{\gamma_{vi}}\right], \tag{39}$$

where$k_{vi1} = diag(k_{viv},\ k_{vi\omega}) > 0$is a constant matrix, $k_{vi2}$and$k_{vi3}$are the diagonal constant matrices, $\Xi_v = [K_{mv},\ K_{cv}, K_{dv}]^T$, $\phi_v = [\|\dot{r}_{vivw}\|, \|r_{vivw}\|, 1,1]^T$ $\|\dot{r}_{vivw}\| = [\|\dot{r}_{viv}\|, \|\dot{r}_{viw}\|]$, $\|r_{vivw}\| = [\|r_{viv}\|, \|r_{viv}\|]$, $\varepsilon_{vi} \geq 0$ and $0 < \gamma_{vi} < 1$ are constants, and $sig(s_{vi})^{\gamma_{vi}} = |s_{vi}|^{\gamma_{vi}}sign(s_{vi})$. The block diagram of the conventional posture and the proposed dual closed-loop posture control system for WMP is described in Fig. 4, where it can be seen that the structure of the proposed posture control system is simpler and easier to be implemented into real experimental system than the conventional posture control system for WMP.

3.5. Design of sliding mode controller of the manipulator

In this section, a sliding mode controller for three-link manipulator shown in Fig. 1 is designed. The separated dynamics of the manipulator from (14) can be expressed as follows:

$$M_m\ddot{q}_m + C_m(q,\dot{q})\dot{q}_m + G_m + F_{dm} = B_m\tau_m, \tag{40}$$

where$F_{dm} = M_{mv}\ddot{q}_v + C_{mv}\dot{q}_v + \tau_{dm}$.

Assumption 3. There are positive real numbersK_{v1}, K_{v2}, andK_{v3}that satisfy the following conditions:

$$\begin{cases} \|M_m\| \leq K_{mm} \\ \|C_m\| \leq K_{cm} \\ \|G_m\| \leq K_{gm} \\ \|F_{dm}\| \leq K_{dm} \end{cases}, \tag{41}$$

where$K_{mm} \in R^{3\times3}$ and$K_{cm} \in R^{3\times3}$ are positive finite diagonal matrices, $K_{gm} \in R^3$ and$K_{dm} \in R^3$ is a positive vector, which are determined through trial and error method.

Assumption 4. There are positive real numbers, Δ_{mm}, Δ_{cm}, Δ_{gm}andΔ_{dm}that satisfy the following conditions:

$$\begin{cases} \|K_{mm} - M_m\| \leq \Delta_{mm} \\ \|K_{cm} - C_m\| \leq \Delta_{cm} \\ \|K_{gm} - G_m\| \leq \Delta_{gm} \\ \|K_{dm} - F_{dm}\| \leq \Delta_{dm} \end{cases}, \tag{42}$$

where$\Delta_{mm}\Delta_{cm}$, $\Delta_{gm}$and$\Delta_{dm}$are the upper bounds of the norm for the off-diagonal coupled term and diagonal estimation error. The joint tracking error, command error, and its derivative are defined as

$$e_m = q_m - q_{md}, \tag{43}$$

$$r_m = \dot{q}_{md} - \Lambda_m e_m, \tag{44}$$

where $q_{md} = [q_{d\theta_1},\ q_{d\theta_2},\ q_{d\theta_3}]^T$ is the desired trajectory, $e_m = [e_{\theta_1},\ e_{\theta_2},\ e_{\theta_3}]^T$, and $\Lambda_m = diag(\Lambda_{m1}, \Lambda_{m2}, \Lambda_{m3}) > 0$ is a constant matrix. The filtered error surface is chosen as

$$s_m = \dot{q}_m - r_m. \tag{45}$$

The dynamic equation (45) can be written as

$$\begin{aligned} M_m\dot{s}_m &= M_m\ddot{q}_m - M_m\dot{r}_m \\ &= -C_m(q_m, \dot{q}_m)\dot{q}_m - G_m(q_m) - F_{dm} + B_m\tau_m - M_m\dot{r}_m \\ &= -M_m\dot{r}_m - C_m(q_m, \dot{q}_m)r_m - F_{dm} - C_m(q_m, \dot{q}_m)s_m + B_m\tau_m. \end{aligned} \tag{46}$$

We select the control law τ_m to satisfy the stability condition, which is given in Section 3, as

$$\tau_m = B_m^{-1}(\tau_{meq} + \tau_{mr} + \tau_{mf}). \tag{47}$$

where

$$\tau_{meq} = -k_{m1}s_m + \Xi_m^T\phi_m, \tag{48}$$

$$\tau_{mr} = -k_{m2}\frac{s_m}{|s_m| + \varepsilon_m}, \tag{49}$$

$$\tau_{mf} = -k_{m3}sig(s_m)^{\gamma_m}, \tag{50}$$

$k_{m1} = diag(k_{m11}, k_{m12}, k_{m13}) > 0$ $k_{m2} = diag(k_{m21}, k_{m22}, k_{m23}) > 0$, $k_{m3} = diag(k_{m31}, k_{m32}, k_{m33}) > 0$ are constant matrices, respectively, $\Xi_m^T = [K_{mm}, K_{cm}, K_{gm}, K_{fm}]$ $\phi_m = [\|\dot{r}_m\|, \|r_m\|, 1,1,1,1,1,1]^T$, $\|\dot{r}_m\| = [\|\dot{r}_{m1}\|, \|\dot{r}_{m2}\|, \|\dot{r}_{m3}\|]$, $\|r_m\| = [\|r_{m1}\|, \|r_{m2}\|, \|r_{m3}\|]$, $\varepsilon_m \geq 0$ and $0 < \gamma_m < 1$ are constants, and $sig(s_m)^{\gamma_m} = |s_m|^{\gamma_m} sign(s_m)$. The controller term τ_{mf}, leads to more rapid response like the WMP controller by selecting proper gains.

Remark 2. In the conventional terminal sliding mode control, the terminal sliding surface is generally defined as $s_m = \dot{e}_m + \Lambda_{m1}sig(e_m)^{\gamma_m}$ [21]. Next, the time derivative of the terminal sliding surface is $\dot{s}_m = \ddot{e}_m + \gamma_m\Lambda_{m1}|e_m|^{\gamma_m - 1}\dot{e}_m$. Then, the singularity problem appears because $\gamma_m\Lambda_{m1}|e_m|^{\gamma_m-1}\dot{e}_m$ goes to infinity due to $-1 < \gamma_m - 1 < 0$ when $e_m = 0$ and $\dot{e}_m = 0$. However, this singularity problem does not exist in the proposed finite time sliding mode control because $s_m = \dot{e}_m + \Lambda_{m1}sig(e_m)^{\gamma_m}$ is not used. The finite control term is considered only in the final controller (47). For this controller, the finite time convergence is proved in the next section.

3.6. Stability analysis of the closed-loop control systems for the WMP and manipulator systems

Lemma 1. [19], [20]. For system (14), the origin of the system is finite time stable if and only if there is a continuous differentiable positive definite time function V and real numbers $c > 0$ and $\gamma \in (0,1)$, in which $\dot{V} + cV^{\gamma} \leq 0$. The upper bound of settling time T_s satisfies the condition

$$T_s \leq \frac{1}{c(1-\gamma)}V^{1-\gamma}. \tag{51}$$

Furthermore, an extended Lyapunov description of finite time stability can be given with the form as

$$\dot{V} + c_1V + c_2V^{\gamma} \leq 0, \tag{52}$$

where $c_1 > 0$ and $c_2 > 0$ are real numbers, and the settling time can be given by

$$T_s \leq \frac{1}{c_1(1-\gamma)}\ln\frac{c_1V^{1-\gamma} + c_2}{c_2}. \tag{53}$$

Lemma 2. [22]. Suppose $a_1, a_2, \ldots, a_n$ and $0 < p < 2$ are all real numbers. The following inequality holds:

$$(a_1^2 + a_2^2 + \cdots + a_n^2)^{p/2} \leq |a_1|^p + |a_2|^p + \cdots + |a_n|^p. \tag{54}$$

Define the Lyapunov function as follows:

$$V = V_{vo} + V_{vi} + V_m \tag{55}$$

where

$$V_{vo} = \frac{1}{2}s_{vo}^T s_{vo}, \tag{56}$$

$$V_{vi} = \frac{1}{2}s_{vi}^T M'_v s_{vi}, \tag{57}$$

$$V_m = \frac{1}{2}s_m^T M_m s_m. \tag{58}$$

The time derivative of (55) based on (28), (38), and (46) is given as

$$\begin{aligned} \dot{V} &= s_{vo}^T\dot{s}_{vo} + s_v^T M_v'\dot{s}_v + \tfrac{1}{2}s_v^T\dot{M}_v' s_v + s_m^T M_m(q_m)\dot{s}_m + \tfrac{1}{2}s_m^T\dot{M}_m(q_m)s_m \\ &= s_{vo}^T\left[J_v(\varphi)J_v^+(\varphi)\left((\dot{q}_{vc} - k_{voe}q_{ve}) - k_{voe}q_{ve} - k_{vo1}s_{vo} - k_{vo2}\frac{s_{vo}}{|s_{vo}| + \varepsilon_{vo}}\right)\right. \\ &\quad \left. - k_{vo3}|s_{vo}|^{\gamma_{vo}}sign(s_{vo}) - \dot{q}_{vc} + k_{voe}q_{ve}\right] \\ &\quad + s_{vi}^T[-M_v'\dot{r}_v - C_v'r_v - F_{dv}' + B_v'\tau_v] + \tfrac{1}{2}s_{vi}^T[\dot{M}_v' - 2C_v']s_{vi} \\ &\quad + s_m^T[-M_m\dot{r}_m - C_m r_m - G_m - F_{dm} + B_m\tau_m] + \tfrac{1}{2}s_m^T[\dot{M}_m - 2C_m]s_m. \end{aligned} \tag{59}$$

Based on the controllers in (29), (39), (47) and property 2, (59) can be expressed as

$$\begin{aligned} \dot{V} &\leq -k_{vo1}s_{vo}^T s_{vo} - k_{vo2}\frac{s_{vo}^T s_{vo}}{|s_{vo}| + \varepsilon_{vo}} - k_{vo3}|s_{vo}|^{\gamma_{vo}+1} - k_{vi1}s_{vi}^T s_{vi} \\ &\quad - k_{vi2}\frac{s_{vi}^T s_{vi}}{|s_{vi}| + \varepsilon_{vi}} - k_{vi3}|s_{vi}|^{\gamma_{vi}+1} \\ &\quad - k_{m1}s_m^T s_m - k_{m2}\frac{s_m^T s_m}{|s_m| + \varepsilon_m} - k_{m3}|s_m|^{\gamma_m+1} \\ &\quad + s_{vi}^T[K_{mv}\|\dot{r}_{vi}\| - M_v'\dot{r}_{vi} + K_{cv}\|r_{vi}\| - C_v'r_{vi} + (K_{dv} - F_{dv}')] \\ &\quad + s_m^T[K_{mm}\|\dot{r}_m\| - M_m\dot{r}_m + K_{cm}\|r_m\| - C_m r_m + (K_{gm} - G_m) + (K_{dm} - F_{dm})] \\ &\leq -k_{vo1}|s_{vo}|^2 - k_{vo2}\frac{|s_{vo}|^2}{|s_{vo}| + \varepsilon_{vo}} - k_{vo3}|s_{vo}|^{\gamma_{vo}+1} - k_{vi1}|s_{vi}|^2 - k_{vi2}\frac{|s_{vi}|^2}{|s_{vi}| + \varepsilon_{vi}} \\ &\quad - k_{vi3}|s_{vi}|^{\gamma_{vi}+1} \\ &\quad - k_{m1}|s_m|^2 - k_{m2}\frac{|s_m|^2}{|s_m| + \varepsilon_m} - k_{m3}|s_m|^{\gamma_m+1} \\ &\quad + |s_{vi}|[\|K_{mv} - M_v'\|\|\dot{r}_{vi}\| + \|K_{cv} - C_v'\|\|r_{vi}\| + \|K_{dv} - F_{dv}'\|] \\ &\quad + |s_m|[\|K_{mm} - M_m\|\|\dot{r}_m\| + \|K_{cm} - C_m\|\|r_m\| + \|K_{gm} - G_m\| \\ &\quad + \|K_{dm} - F_{dm}\|] \\ &= -k_{vo1}|s_{vo}|^2 - k_{vo2}\frac{|s_{vo}|^2}{|s_{vo}| + \varepsilon_{vo}} - k_{vo3}|s_{vo}|^{\gamma_{vo}+1} - k_{vi1}|s_{vi}|^2 - k_{vi2}\frac{|s_{vi}|^2}{|s_{vi}| + \varepsilon_{vi}} \\ &\quad - k_{vi3}|s_{vi}|^{\gamma_{vi}+1} \\ &\quad - k_{m1}|s_m|^2 - k_{m2}\frac{|s_m|^2}{|s_m| + \varepsilon_m} - k_{m3}|s_m|^{\gamma_m+1} \\ &\quad + |s_{vi}|[\Delta_{mv}\|\dot{r}_{vi}\| + \Delta_{cv}\|r_{vi}\| + \Delta_{dv}] \\ &\quad + |s_m|[\Delta_{mm}\|\dot{r}_m\| + \Delta_{cm}\|r_m\| + \Delta_{gm} + \Delta_{dm}] \\ &= -k_{vo1}|s_{vo}|^2 - k_{vo3}|s_{vo}|^{\gamma_{vo}+1} - k_{vi1}|s_{vi}|^2 - k_{vi3}|s_{vi}|^{\gamma_{vi}+1} - k_{m1}|s_m|^2 \\ &\quad - k_{m3}|s_m|^{\gamma_m+1} \end{aligned}$$

Table 1
Parameters of the WMP and manipulator systems.

Symbol	Parameter	Value
m_p, m_w, m_1, m_2, m_3	mass of body, wheel, link1, 2, 3	$5kg$,$0.58kg$, $0.5kg$$0.5kg$$0.5kg$
l_1, l_2, l_3	length of link1, 2, 3	$110mm$, $255nm$, $120mm$
d	the distance between the point P and wheel	$0.145m$
r	radius of wheel	$0.075m$

$$- |s_{vi}|\left(\frac{k_{vi2\min}|s_{vi}|}{|s_{vi}|+\varepsilon_{vi}} - \rho_{vi}\right) - |s_m|\left(\frac{k_{m2\min}|s_m|}{|s_m|+\varepsilon_m} - \rho_m\right) \tag{60}$$

where$k_{vi2\min} = \lambda_{\min}(k_{vi2})k_{m2\min} = \lambda_{\min}(k_{m2})$, $\rho_{vi} = \Delta_{mv}\|\dot{r}_{vi}\| + \Delta_{cv}\|r_{vi}\| + \Delta_{dv}$ $\rho_m = \Delta_{mm}\|\dot{r}_m\| + \Delta_{cm}\|r_m\| + \Delta_{gm} + \Delta_{dm}$. If$k_{vi2\min}$ and $k_{m2\min}$ are selected such that$k_{vi2\min}|s|_{vi} \geq \rho_{vi}(|s_{vi}| + \varepsilon_{vi})$ and$k_{m2\min}|s|_{mi} \geq \rho_m(|s_m| + \varepsilon_m)$are guaranteed, it follows that

$$\dot{V} = \dot{V}_{vo} + \dot{V}_{vi} + \dot{V}_{vm}$$

$$\leq -k_{vo1}|s_{vo}|^2 - k_{vo3}|s_{vo}|^{\gamma_{vo}+1} - k_{vi1}|s_{vi}|^2 - k_{vi3}|s_{vi}|^{\gamma_{vi}+1} - k_{m1}|s_m|^2 - k_{m3}|s_m|^{\gamma_m+1} \tag{61}$$

Based on Lemma 2, (61) can be rewritten as

$$\dot{V} \leq -k_{vo1}s_{vo}^2 - k_{vo3}(s_{vo}^2)^{(\gamma_{vo}+1)/2} - k_{vi1}s_{vi}^2 - k_{vi3}(s_{vi}^2)^{(\gamma_{vi}+1)/2} - k_{m1}s_m^2 - k_{m3}(s_m^2)^{(\gamma_m+1)/2}. \tag{62}$$

From the definition of (57) and (58) with the fact that$\|s\| \leq |s|$, it follows that

$$V_{vi} = \frac{1}{2}s_{vi}^T M_v' s_{vi} \leq \frac{1}{2}\lambda_{\max}(M_v')s_{vi}^T s_{vi} = \frac{1}{2}\lambda_{\max}(M_v')\|s_{vi}\|^2 \leq \frac{1}{2}\lambda_{\max}(M_v')|s_{vi}|^2,$$

$$V_m = \frac{1}{2}s_m^T M_m s_m \leq \frac{1}{2}\lambda_{\max}(M_m)s_m^T s_m = \frac{1}{2}\lambda_{\max}(M_m)\|s_m\|^2 \leq \frac{1}{2}\lambda_{\max}(M_m)|s_m|^2. \tag{63}$$

Based on Lemma 2, Based on Lemma 2, (61), (62), and (63), the following expression can be obtained:

$$\dot{V}_{vo} \leq -c_1 V_{vo} - c_2 V_{vo}^{\mu_1}, \tag{64}$$

$$\dot{V}_{vi} \leq -c_3 V_{vi} - c_4 V_{vi}^{\mu_2}, \tag{65}$$

$$\dot{V}_m \leq -c_5 V_m - c_6 V_m^{\mu_3}, \tag{66}$$

with$c_1 = 2k_{vo1}$, $c_2 = 2^{(\gamma_{vo}+1)/2}k_{vo3}c_3 = \frac{2k_{vi1}}{\lambda_{\max}(M'v)}$, $c_4 = \frac{2^{(\gamma_{vi}+1)/2}k_{vi3}}{\lambda_{\max}(M'v)}$

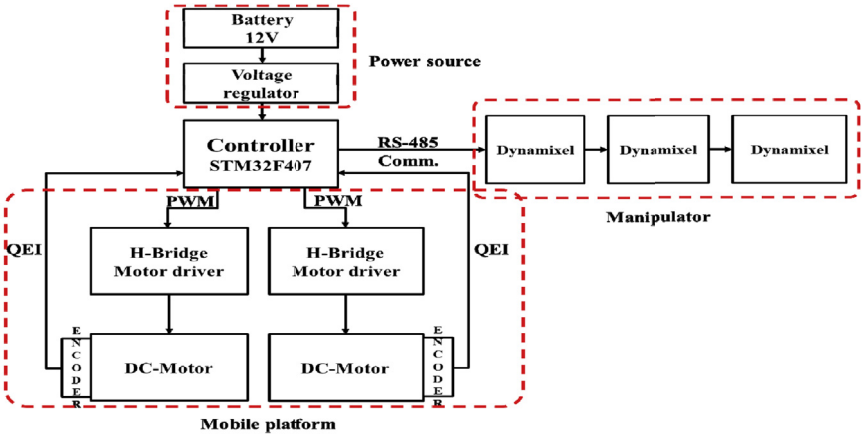

(a)

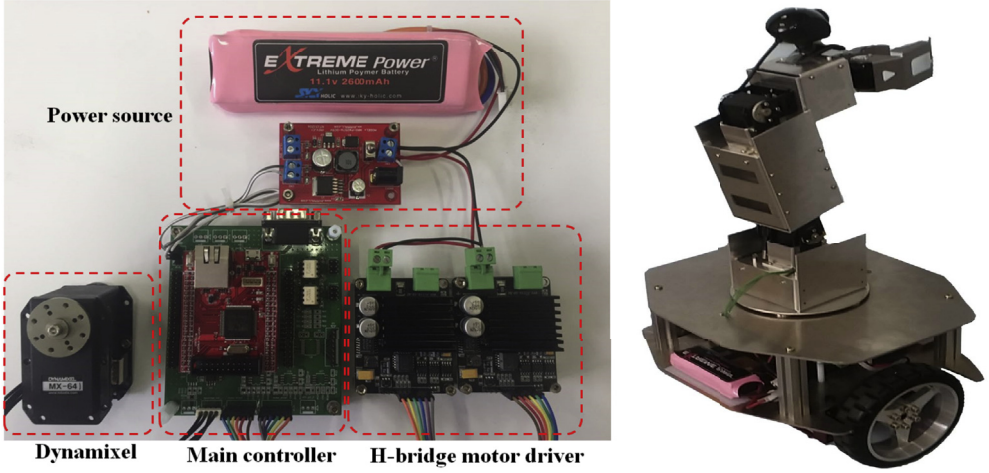

(b)

Fig. 9. Hardware system of the mobile manipulator. (a) Diagram of the main control board and sensor system.

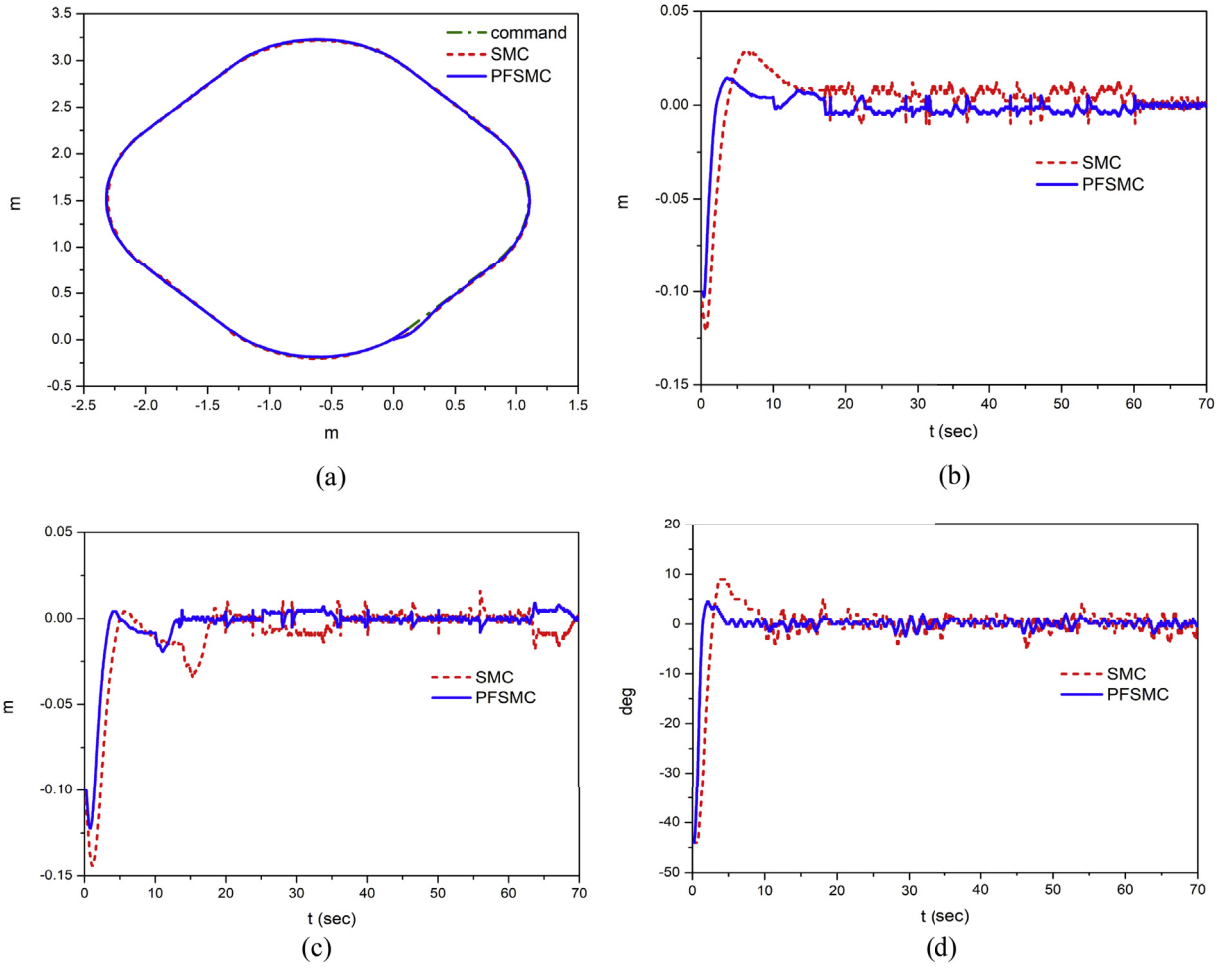

Fig. 10. Experimental results for the linear and rotational motion command input of the SMC and PFSMC systems: (a) Position tracking output. (b) X-direction tracking error. (c) Y-direction tracking error. (d) Angular tracking error.

Table 2
RMS values for the tracking error of the WMP.

System	X-direction (m)	Y-direction (m)	φ-direction (rad)
SMC (100%)	0.036 (100%)	0.007 (100%)	0.017 (100%)
FSMC (60%)	0.018 (50%)	0.004 (57%)	0.012 (71%)

$c_5 = \frac{2k_{m1}}{\lambda_{\max}(M_m)}$, $c_6 = \frac{2^{(\gamma_m+1)/2}k_{m3}}{\lambda_{\max}(M_m)}\mu_1 = (\gamma_{vo}+1)/2\mu_2 = (\gamma_{vi}+1)/2$, and$\mu_3 = (\gamma_{vm}+1)/2$. Then, using Lemma 1, the finite convergence times in the WMP and manipulator systems are given respectively as

$$T_{svo} \le \frac{1}{c_1(1-\mu_1)} \ln \frac{c_1 V^{1-\mu_1} + c_2}{c_2}, \tag{67}$$

$$T_{svi} \le \frac{1}{c_3(1-\mu_2)} \ln \frac{c_3 V_{vi}^{1-\mu_2} + c_4}{c_4}, \tag{68}$$

$$T_{sm} \le \frac{1}{c_5(1-\mu_3)} \ln \frac{c_5 V_m^{1-\mu_3} + c_6}{c_6}. \tag{69}$$

The final finite convergence time of the whole system is determined as

$$T_s = \max(T_{svo}, T_{svi}, T_{sm}), \tag{70}$$

i.e., the final convergence time is the longest time among each convergence time.

Remark 3. The finite time sliding mode controllers designed in (29), (39), and (47) become the normal sliding mode controllers if the finite time control terms, $-k_{vo3}sig(s_{vo})^{\gamma_{vo}}$– $k_{vi3}sig(s_{vi})^{\gamma_{vi}}$, and– $k_{m3}sig(s_m)^{\gamma_m}$, are removed from each controller. In this case, the final reaching time can be obtained asmax(T_{rv}, T_{rm}), where$T_{rv} \le |s_v(0)|/K_v$, $T_{rm} \le |s_m(0)|/K_m$, $s_{rv} = [s_{vo}\ \ s_{vi}]^T$, $K_v$and$K_m$are constants defined properly from WMR and manipulator control systems.

4. Simulation and experimental application

In this section, simulation and experiment results for posture control of the WMP and joint position control of manipulator. The dynamic parameters of mobile manipulator are listed in Table 1. The command input of the WMP system is generated as the linear and rotary motion shown in Fig. 5, where Fig. 5 (a) is decomposed into Fig. 5 (b) and (c).

Next, to generate the link motions, the inverse kinematics for the end-effector need to be obtained. Thus, based on the kinematic configuration of three links in Fig. 1 (b), the following relations can be derived:

$$\begin{aligned} x_e &= (l_2 \sin\theta_2 + l_3 \sin(\theta_2+\theta_3))\cos\theta_1, \\ y_e &= (l_2 \sin\theta_2 + l_3 \sin(\theta_2+\theta_3))\sin\theta_1, \\ z_e &= l_1 + l_2\cos\theta_2 + l_3\cos(\theta_2+\theta_3), \end{aligned} \tag{71}$$

where$(x_e, y_e, z_e)$is the coordinate of the end-effector with respect to robot frame point C. The inverse kinematics for the 3-DOF manipulator

can be obtained as follows:

$$\theta_1 = \text{atan2}\left(\frac{y_e}{x_e}\right),$$

$$\theta_2 = \min(\theta_2', \theta_2'),$$

$$\theta_3 = \text{acos}\left(\frac{z_e - l_1 - l_2\cos\theta_2}{l_3}\right) - \theta_2, \tag{72}$$

$$\text{where}\theta_2' = \text{asin}\left(\frac{(z_e-l_1)^2 + x_e^2 + y_e^2 + l_2^2 + l_3^2}{2l_2\sqrt{x_e^2+y_e^2+(z_e-l_1)^2}}\right) - \text{atan2}\left(\frac{z_e-l_1}{\sqrt{x_e^2+y_e^2}}\right),$$

$$\theta_2' = 2\text{atan2}\left(\frac{\sqrt{x_e^2+y_e^2}}{x_e}\right) - \theta_2', \text{and} x_e \neq 0.$$

In this paper, the end-effector motion is generated as the following Fig. 6 (a). Fig. 6 (b) indicates the joint angles of each joint based on (82), where $x_e = 400mm y_e = -195mm + 19.5tmm$, and$z_e = -120\sin(0.016(y_e + 195))mm + 130mm$.

To show the comparative control performance of the proposed control scheme, two controllers are designed: the proposed dual closed-loop finite-time sliding mode controller (PFSMC) and the dual closed-loop sliding mode controller (SMC). The selected control gains between two controllers were same except the gains of the finite-time control term. In the simulation, the following control parameters were selected: $k_{voe} = diag(0.5, 0.5, 0.5)k_{vo1} = diag(2,2,2)k_{vo2} = diag(10,10,5)k_{vo3} = diag(4,4,4)k_{vi1} = diag(1,1)k_{vi2} = diag(2.5, 2.5)k_{vi3} = diag(2,2)k_{m1} = 0.2$ $k_{m2} = 0.75k_{m3} = 0.9\Lambda_{vi} = diag(0.5, 0.5)\Lambda_m = diag(3,3,1)\varepsilon_{vi} = 0.1\varepsilon_{vo} = 0.1$ $\varepsilon_{vi} = 0.1\varepsilon_m = 0.1\gamma_{vo} = 0.5\gamma_{vi} = 0.5\gamma_m = 0.5K_{mv} = diag(8.16, 0.33)$ $K_{cv} = diag(1, 0)K_{dv} = diag(0.15, 0.01)K_{mm} = diag(0.5, 0.5, 0.5)$ $K_{cm} = diag(0,0.063, 0.075)K_{gm} = diag(0,5.53, 4.91)$, $K_{fm} = diag(0.057, 0.56, 0.125).k_{vo1}k_{vo1}$, and$k_{m1}$ relate the convergence speed from any initial state point to the sliding surface. $k_{vo2}k_{vi2}k_{m2}$ ε_{vi}, ε_{vo}, and$\varepsilon_m$relate staying in sliding surface of each state and determine robustness of the controller. $k_{vo3}k_{vi3}$, $k_{m3}\gamma_{vo}$,γ_{vi},andγ_m determine the convergence speed to zero steady-state error. In this paper, the controller gains were selected by these routes and can be varied according to the change of the required specification. Some parameters among these control parameters were a little changed in experiment.

4.1. Simulation application

Simulation for the mobile manipulator system as shown in Fig. 1 was executed to demonstrate the performance of the proposed dual closed-loop finite time sliding mode controller. In simulation, all control gains were tuned for the nominal masses of each link given in Table 1. To check robustness to uncertainty of the proposed control system, the mass of the link 3, which corresponds to the end-effector of the manipulator, increased as four times of its nominal value ($0.5kg$).

In Fig. 7 (a), the tracking results of the WMP for the linear and rotary posture command inputs are presented in the SMC and the PFSMC systems. Fig. 7 (b)-(c) show the motion tracking errors, where comparing with the results of both systems in Fig. 7, it is seen that the proposed control system has reasonable tracking performance. In Fig. 8, simulation results for manipulator system of the SMC and PFSMC systems are presented, where the PFSMC control system shows more robust control performance than those of the SMC system for the inertia

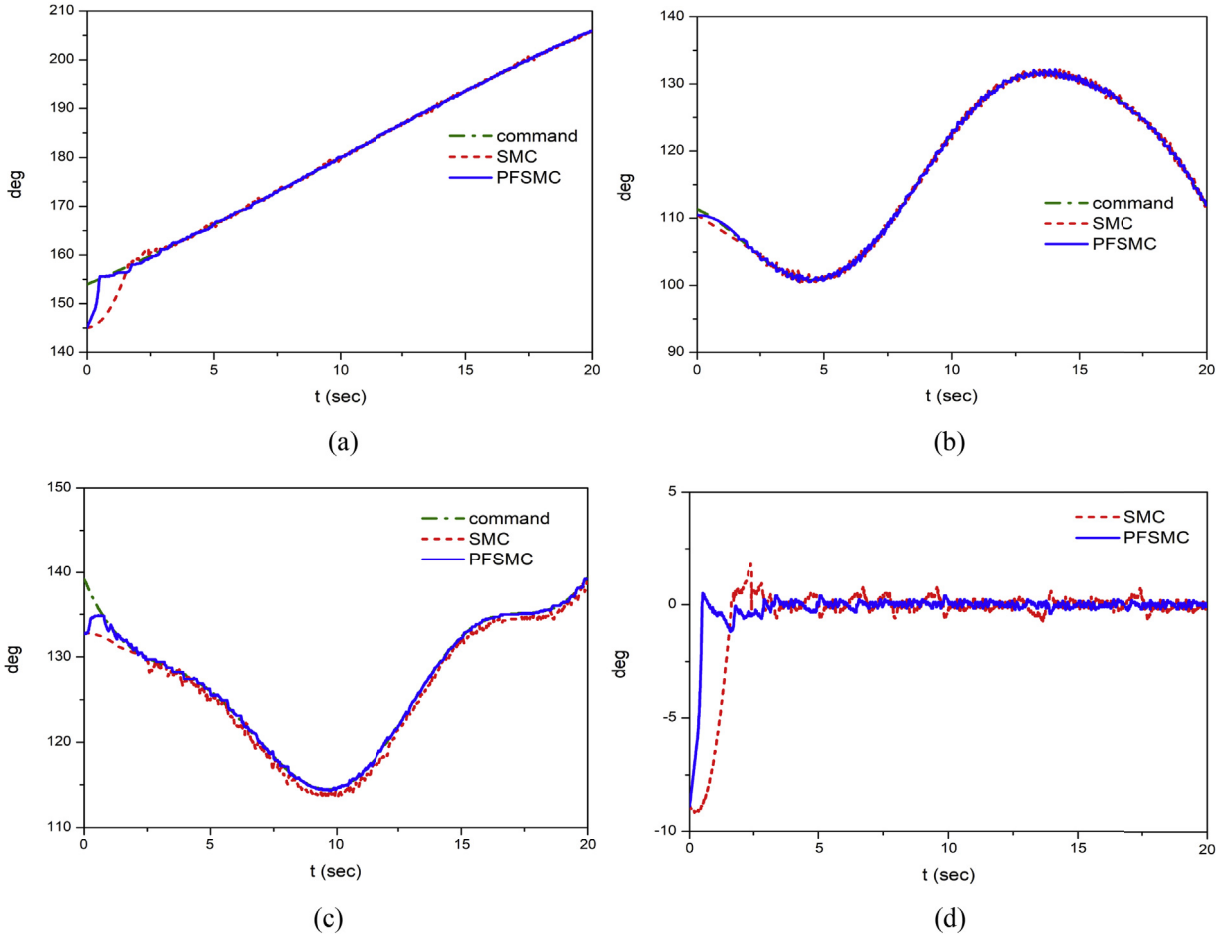

Fig. 11. Experimental results for manipulator system of the SMC and PFSMS systems. (a) Tracking result of link 1. (b) Tracking result of link 2. (c) Tracking result of link 3. (d) Tracking error of link 1. (e) Tracking error of link 2. (f) Tracking error of link 3. (g) Control input of joint 1. (h) Control input of joint 2. (i) Control input of joint 3.

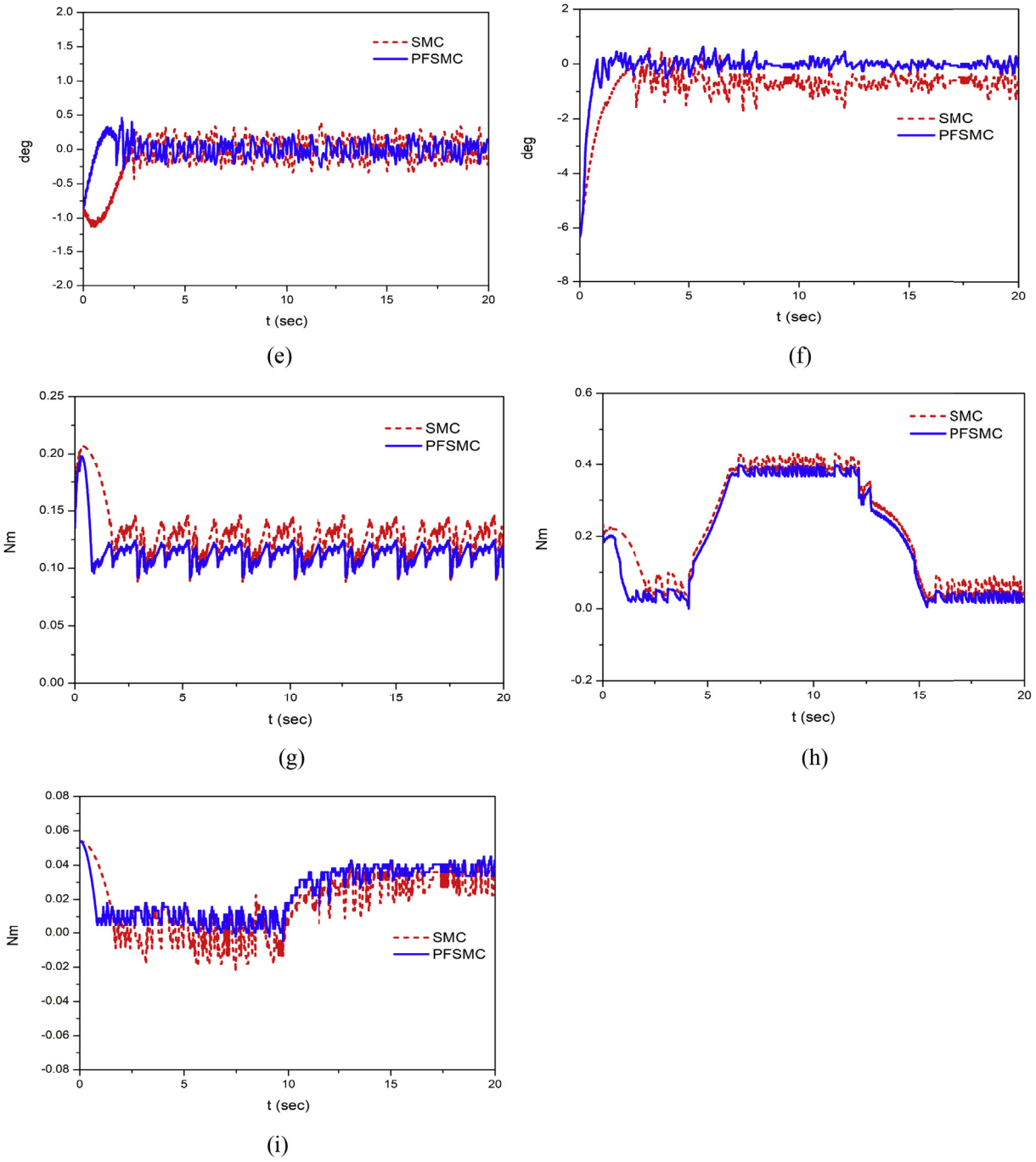

Fig. 11. (*continued*)

change of link 3 due to adding extra mass to end-effector. In the response in link 3 shown in Fig. 8 (c), the steady-state error of the PFSMC system is smaller than that of the SMS system.

4.2. Experimental application

In this section, experiment results for mobile manipulator of the SMC system and PFSMC systems are presented for comparison of control performance. The hardware equipment of the proposed mobile manipulator system is illustrated in Fig. 9, where the STM32F407 ARM microprocessor was adopted as the main controller, DC motor system is used in the mobile wheel drive system, and dynamixel motor system [23] is built for manipulator control. Data acquisitions were carried out through the wireless ZigBee communication method. The data of x and y axes were obtained from 9-DOF Razor IMU sensor. 9-DOF IMU sensor consists of gyroscope, accelerometer, and magnetometer. The odometry information is used to estimate the mobile robot's position relative to its origin. The odometry data of x and y axes were calculated by combining the data of gyroscope, accelerometer, and encoder. The data of$\theta_1\theta_2$, and $\theta_3$were obtained from dynamixel encoder.

Experimental results of the WMP for the linear and rotary posture command are presented in Fig. 10. The tracking results are shown in Fig. 10 (a) and Fig. 10 (b), (c), and (d) show the tracking errors in each axis, where it can be seen that the convergence time of the PFSMC system is shorter than those of the SMC system. As shown in Table 2, the values of the root mean square (RMS) error in the PFSMC system are averagely 60% smaller over the SMC system.

Experimental results of manipulator for the link motion command

Table 3
RMS values for the tracking error of manipulator.

System	Link1 (deg)	Link2 (deg)	Link3 (deg)
SMC (100%)	2.042 (100%)	0.313 (100%)	1.147 (100%)
FSMC (52%)	1.026 (50%)	0.146 (47%)	0.680 (59%)

given in Fig. 6 are presented in Fig. 11. Fig. 11 (a), (b), and (c) show the tracking results of each link and the tracking errors are presented in Fig. 11 (d), (e), and (f), where the convergence time of the PFSMC system is also shorter than those of the SMC system. In addition, the steady-state error of the PFSMC system in link 3 is smaller than that of the SMC system. Thus, the PFSMC system is more robust over the SMC system for uncertainty as well as having faster response. As shown in Table 3, the values of the root mean square (RMS) error in the PFSMC system are averagely 52% smaller over the SMC system. The control torques in the joints are presented in Fig. 11 (g), (h), and (i).

5. Conclusion

In this paper, a dual closed-loop finite-time SMC system for the three-wheeled and three-link mobile manipulator compared to the conventional sliding mode control were proposed. The first achievement of this paper is to obtain fast and intuitive posture trajectory generation of the WMP and robust joint tracking performance of manipulator. For this achievement, a sliding mode surface based virtual velocity command in outer loop was generated instead of the perfect velocity control of backstepping control. The second one is to derive simpler decoupled dynamics between mobile platforms and manipulators than full-coupled model based ones by considering the Euler-Lagrange equation and partial Newtonian method. Next, as the third achievement, two dynamic finite-time sliding mode controller in inner loop of the WMP and manipulator systems were design to compensated velocity gaps between the virtual velocity command and real velocity and joint position tracking errors and finite-time control terms were considered to obtain faster convergence time and stronger robustness. Comparative simulation and experimental results with other control systems supported the effectiveness of the proposed control method.

Acknowledgements

This work has supported by the National Research Foundation of Korea (NRF) grant funded by the Korea government (MSIT) (No. NRF-2018R1A2B6005128)

References

[1] Yamamoto Y, Yun X. Coordinating locomotion and manipulation of a mobile manipulator. IEEE Trans Automat Contr 1994;39(6):1326–32.
[2] Chung JH, Velinsky SA. Robust interaction control of a mobile manipulator – dynamic model based coordination. J Intell Rob Syst 1999;26:47–63.
[3] Lin S, Goldenberg AA. Neural-network control of mobile manipulators. IEEE Trans Neural Network 2001;12(5):1121–33.
[4] Tsai CC, Cheng MB, Lin SC. Dynamic modeling and tracking control of a non-holonomic wheeled mobile manipulator with dual arms. J Intell Rob Syst 2006;47:317–40.
[5] Li Z, Ge SS, Wang Z. Robust adaptive control of coordinated multiple mobile manipulators'. Mechatronics 2008;18:239–50.
[6] Cheng MB, Su WC, Tsai CC. Robust tracking control of a unicycle-type wheeled mobile manipulator using a hybrid sliding mode fuzzy neural network. Int J Syst Sci 2012;43(3):408–25.
[7] Li Z, Yang C, Tang Y. Decentralized adaptive fuzzy control of coordinated multiple mobile manipulators interacting with non-rigid environments. IET Control Theory Appl 2013;18:2885–99.
[8] Fierro R, Lewis FL. Control of a nonholonomic mobile robot: backstepping kinematics into dynamics. J Rob Syst 1997;14(3):149–63.
[9] Pourboghrat F, Karlsson MP. Adaptive control of dynamic mobile robots with nonholonomic constraints. Comput Electr Eng 2002;28:241–53.
[10] Kim MS, Shin JH, Hong SG, Lee JJ. Designing a robust dynamic controller for nonholonomic mobile robots under modeling uncertainty and disturbances. Mechatronics 2003;13:507–19.
[11] Chen CY, Li THS, Yeh YC, Chang CC. Design and implementation of an adaptive sliding-mode dynamic controller for wheeled mobile robots. Mechatronics 2009;29:156–65.
[12] Yue M, Hu P, Sun W. Path following of a class of non-holonomic mobile robot with underactuated vehicle body. IET Control Theory Appl 2010;4(10):1898–904.
[13] Slotine JJ, Li W. Applied nonlinear control. New Jersey: Prentice Hall; 1991.
[14] Dong L, Tang WC. Adaptive backstepping sliding mode control of flexible ball screw drives with time-varying parametric uncertainties and disturbances. ISA Trans 2014;53(1):110–6.
[15] Wang J, Zong Q, Su R, Tian B. Continuous high order sliding mode controller design for a flexible air-breathing hypersonic vehicle. ISA Trans 2014;53(3):690–8.
[16] Abjadi NR. Sliding-mode control of a six-phase series/parallel connected two induction motors drive. ISA Trans 2014;53(6):1847–65.
[17] Liang C, Li Y. Attitude tracking control based on adaptive sliding mode technique with double closed loop for spacecraft near small body. IEEE 17th Inter. Conference Comput Sci Eng 2015:78–82.
[18] Li X, Zhao H, Zhao X, Ding H. Dual sliding mode contouring control with high accuracy contour error estimation for five-axis CNC machine tools. Int J Mach Tool Manufact 2016;108:74–82.
[19] Bhat SP, Bernstein DD. Finite-time stability of continuous autonomous systems. SIAM J Contr Optim 2000;38(3):751–66.
[20] Hong Y, Huang Y. On an output finite-time stabilization problem. IEEE Trans. A. C 2001;46(4):305–9.
[21] Yu X, Man Z. Fast terminal sliding-mode control design for nonlinear dynamical systems, IEEE Tran. Circuit and Sys.-I: Fundamental Theory Appl. 2002;49(2):261–4.
[22] Barambose O, Etxeberria V. Energy-based approach to sliding mode composite adaptive control for rigid robots with finite error convergence time, Int. J. Control 2002;75(5):352–9.
[23] Dynamixel MX-series, MX ROBOTIS INC, USA.